Investigation of Lanthanum Scintillators for 3-D PET

S. Surti, *Member, IEEE*, J. S. Karp, *Senior Member, IEEE*, G. Muehllehner, *Fellow, IEEE*, and P. S. Raby

***Abstract*—The main thrust for this work is the investigation and design of a positron emission tomography (PET) scanner based on new Lanthanum Halide scintillators. In three–dimensional (3-D) PET the major limitations are scanner dead-time and ability to reject randoms and scatter. Therefore, to reach the full potential of 3-D PET requires a scintillator with good timing resolution and good energy resolution. The new Lanthanum Halide scintillators have very fast decay and very high light output which leads to timing resolution and energy resolution that are both superlative. For application to PET, the authors have constructed pixels with dimensions $4 \times 4 \times 30$ mm^3 and have measured energy resolution of 4.6% (fwhm) at 662 keV and a timing resolution (fwhm) of 350 ps, in coincidence with a plastic scintillator. Using a detector based on $LaBr_3$, a 3-D PET scanner with 90 cm diameter and 25 cm axial extent is predicted to achieve a sensitivity of 1400 kc/s/μCi/cc and a peak NEC count-rate of 120 kc/s using the NEMA NU2-2001 standard. Further, the excellent timing resolution opens the possibility of measuring time-of-flight with sufficient accuracy to reduce the noise propagation during image reconstruction, thus leading to a significant gain in signal-to-noise. Assuming a system timing resolution of 500 ps, one can expect the effective NEC to increase by a factor of 3 for a thin patient (20 cm diameter) and a factor 6 for a very heavy patient (40 cm diameter). Thus, even with lower stoping power than other PET scanners, the combination of excellent energy resolution and timing resolution of $LaBr_3$ can potentially lead to a very significant improvement in PET performance.**

I. Introduction

THERE HAS been considerable research and development of inorganic scintillators for positron emission tomography (PET) imaging over the past several decades [1] and the search for the ideal scintillator is intensifying. The ideal scintillator has high light output, high stopping power, and fast decay time. Although far from ideal, both NaI(Tl) and BGO have been used in PET for a long period of time—almost 30 years for NaI(Tl) and 25 years for BGO [2]—and both continue to be incorporated in commercial PET instruments capable of high performance. Nevertheless, LSO and GSO have drawn much attention recently, as both can lead to higher performance, particularly for three–dimensional (3-D) instrument, for brain imaging [3], [4] as well as whole-body imaging as demonstrated by the Siemens/CTI *Accel* and Philips *Allegro*. Table I compares properties of scintillators. The combination of stopping power, timing, and energy resolution makes LSO and GSO scintillators very attractive for 3-D PET despite the high cost. As production capacity increases, it is possible that these scintillators will continue to get less expensive, although it is unlikely that either LSO or GSO will reach the low cost of NaI(Tl) and BGO, due to the higher melting point (2000°C) and difficulty in growing large boules.

TABLE I
COMPARISON OF PROPERTIES OF SCINTILLATORS FOR PET. ENERGY RESOLUTION TAKEN AT 662 KEV. DATA ARE COLLECTED FROM [5] AND [1]

Scintillator	τ (ns)	μ (cm^{-1})	ΔE/E (%)	Relative light output (%)
NaI(Tl)	230	0.35	6.6	100
BGO	300	0.95	10.2	15
CsF	3	0.39	18.0	5
BaF_2	2	0.45	11.4	5
GSO	60	0.70	8.5	25
LSO	40	0.86	10.0	75
LuAp	18	0.95	$\sim$15	30
LPS	30	0.70	$\sim$10	73
$LaCl_3$	26	0.36	3.3	120
$LaBr_3$	35	0.47	2.9	160

Recently, we have become interested in the development of a new class of fast scintillators ($LaCl_3$ and $LaBr_3$) that have been reported on by van Loef at Delft University in the last two years [6]–[8]. The low melting point of the Lanthanum scintillators [800–900 °C, similar to NaI(Tl)] suggests that in the long run these scintillators can be cost-effective compared to GSO and LSO. Table I shows that the stopping power of $LaCl_3$ is similar to that of NaI(Tl), while the stopping power of $LaBr_3$ is higher, an advantage for PET. Both Lanthanum scintillators have very high light output, higher than NaI(Tl), the gold standard, and outstanding energy resolution. The extremely good energy resolution is due to the very high light output as well as very small nonproportionality of the scintillator [1], [9]. The excellent energy resolution of the Lanthanum scintillators potentially allows the use of a very high energy lower level discriminator (ELLD) level to reject the majority of scatter and randoms which are often the limiting factor of image quality for 3-D PET (no inter-plane septa). In addition, the fast decay and excellent timing resolution will minimize deadtime and random coincidences, which is key for 3-D PET. We have designed an Anger-logic detector with continuous optical coupling and based upon Lanthanum scintillators to take full advantage of the high light output, which enables us to use long and narrow scintillators so as to achieve both high sensitivity and high spatial resolution. Further, the combination of very high light output and fast decay opens the possibility of measuring time-of-flight with sufficient accuracy, which can potentially provide a very significant additional gain in signal-to-noise ratio

Manuscript received December 3, 2002; revised March 21, 2003. This work was supported by the U.S. Department of Energy under Grant DE-FG02-88ER60642 and by a research agreement with Saint Gobain Crystals & Detectors.

S. Surti and J. S. Karp are with the Department of Radiology, University of Pennsylvania, Philadelphia, PA 19104 USA.

G. Muehllehner is with the Philips Medical Systems, Philadelphia, PA 19104 USA.

P. S. Raby is with the Saint-Gobain Crystals & Detectors, Newbury, OH 44065 USA.

Digital Object Identifier 10.1109/TNS.2003.812450

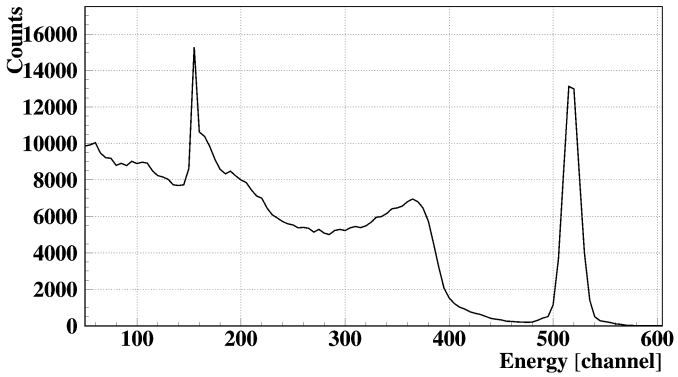

Fig. 1. Energy spectrum of $LaBr_3$.

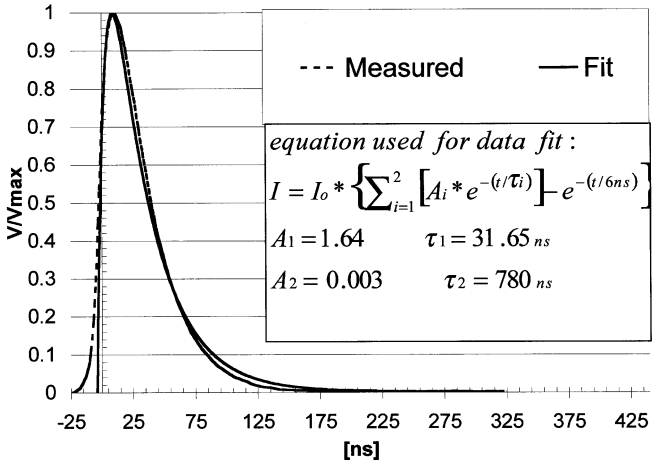

Fig. 2. Pulse shape of $LaBr_3$.

(SNR) and image quality, particularly for large patients where image quality normally degrades in PET.

II. Measurements

Initial measurements show a 3.25% energy resolution (at 662 keV) for a single $LaBr_3$ crystal (10 mm diameter $\times$ 6 mm long coupled to a Photonis XP2020 PMT, Fig. 1) with a decay time close to 32 ns and a very small component with longer decay time (Fig. 2). This was achieved by varying the Cerium content, as the first results reported by the group at Delft showed a decay spectrum with a much longer tail, which would potentially cause a problem in PET at high count-rates. Further, $LaBr_3$ has an excellent time resolution, due to its combination of fast decay and high light output. We requested $4 \times 4 \times 30$ mm^3 crystal samples since these represent appropriate dimensions for a PET detector requiring high sensitivity (thick crystal) and spatial resolution (narrow crystal). Recent measurements with this $4 \times 4 \times 30$ mm^3 $LaBr_3$ crystal showed very promising results of 4.6% energy resolution at 662 keV and a timing resolution of 350 ps at 511 keV in coincidence with plastic. These results show that the Lanthanum scintillators are capable of maintaining the timing and energy resolution properties in long and narrow crystals, which is needed to achieve high sensitivity and spatial resolution in PET.

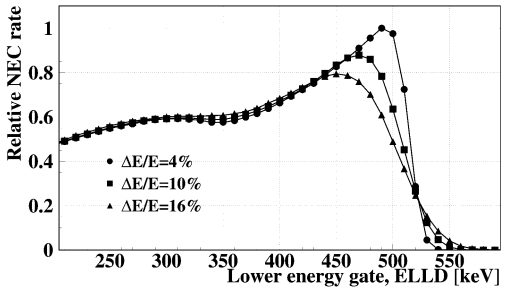

(a)

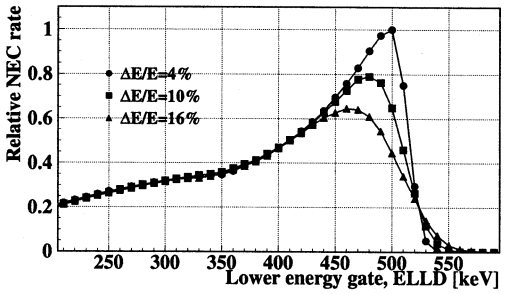

(b)

Fig. 3. (a) Calculated relative NEC as a function of system energy resolution and energy lower level discriminator (ELLD) for a phantom 20 cm diameter and 70 cm long. (b) Same, but for a phantom 40 cm diameter and 70 cm long.

III. Benefit of Good Energy Resolution

In order to study the benefit of energy resolution in patient studies, we calculated relative NEC curves for a 20 cm diameter by 70 cm long phantom (NEMA NU2–2001) representing a slim patient, as well as a 40 cm diameter by 70 cm long phantom representing a larger patient. Relative NEC as shown previously [10] is given by

$$\text{Relative } NEC_{(\text{ELLD})} = (1 - SF_{(\text{ELLD})})^2 \times \epsilon^2_{(\text{ELLD})}$$

where SF is the scatter fraction as defined by NEMA, ELLD is the lower energy gate, and ϵ is the fraction of single events which lie above the ELLD. Relative NEC is the component of NEC value which is dependent only on the ELLD setting. These calculations assume no dead-time, a constant activity concentration, and similar energy spectra for single and coincident events. Fig. 3 shows relative NEC rates as a function of ELLD for a fixed activity concentration and varying energy resolution from 4% to 16%. These calculations were performed for a 3-D whole-body scanner design with a 90 cm diameter, axial FOV of 25 cm, and $4 \times 4 \times 30$ mm^3 $LaBr_3$ crystals.

The cases calculated in Fig. 3 are illustrative of scanners with different energy resolutions. We chose 16%, 10%, and 4% because these three values represent the system energy resolution that we have achieved with GSO and NaI(Tl) and the best possible energy resolution of a $LaBr_3$ scanner. For all three cases the same geometry was assumed, only the energy resolution and energy thresholds were changed. It is interesting to note that for a slim patient (20 cm diameter phantom), the improvement in NEC with better energy resolution is only about 25%. With heavier patients, on the other hand, the relative NEC improves from 0.64 to 1.0, an improvement of about 50%, as the ELLD

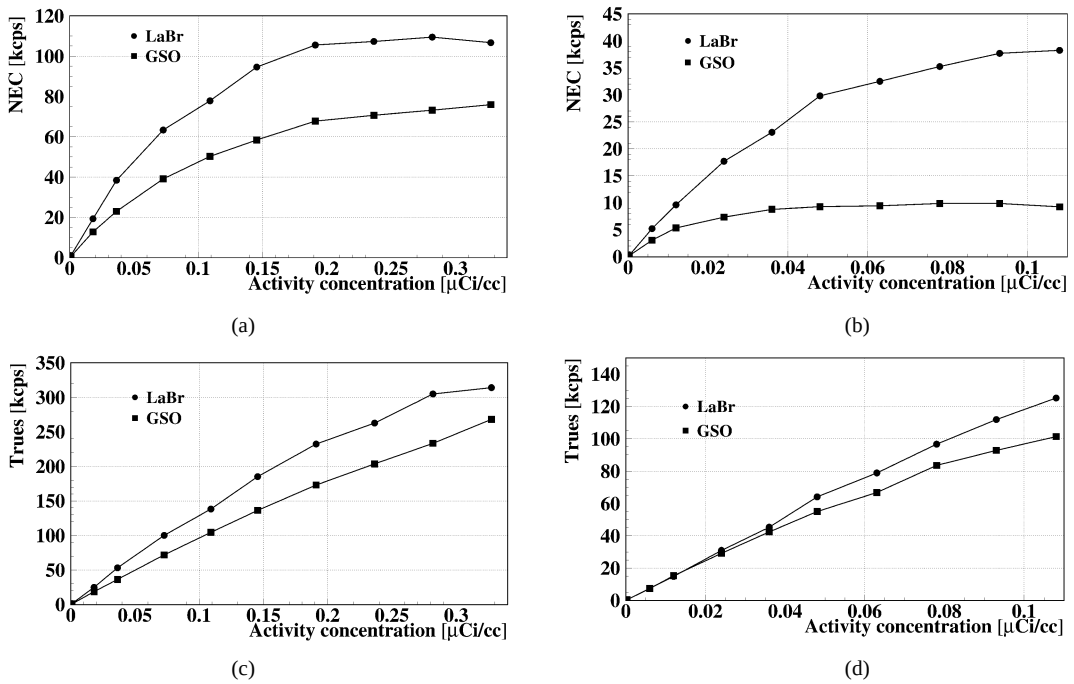

Fig. 4. (a), (b) NEC and (c), (d) true count-rate curves calculated by HCRSim for different whole-body scanners. GSO scanner uses 20 mm thick crystals with an axial length of 18 cm. $LaBr_3$ scanner uses 30 mm thick crystals with a 25 cm axial length. NEC rates are calculated for a non-TOF scanner. (a), (c) 20 cm by 70 cm phantom and (b), (d) 40 cm by 70 cm phantom. Note the vertical scale change.

TABLE II
INTERACTION PROBABILITIES FOR DIFFERENT SCINTILLATORS AT 511 KEV. CRYSTAL LENGTH IS NOTED

Scintillator/length (mm)	GSO/20	$LaBr_3$/30
μ (cm^{-1})	0.70	0.47
Singles photopeak efficiency (%)	0.51	0.47
Coincidence photopeak efficiency (%)	0.26	0.22

is raised to achieve peak NEC. Since heavy patients are particularly difficult to image and typically result in noisy low contrast images, the benefit of better energy resolution is most significant here.

IV. COUNT-RATE SIMULATIONS

We have performed high count rate simulation program (HCRSim) [11], [12] calculations, which model pulse pileup and deadtime within our scanners, to investigate the potential improvements that can be achieved with a $LaBr_3$ crystal in a whole-body scanner design. This simulation specifically takes into account the light spread within the the detector, as well as the signal width, to obtain the scanner deadtime as a function of activity concentration within a cylindrical phantom. The scanner size was modeled on the C-PET geometry with a diameter of 90 cm and axial length of 25 cm. The $LaBr_3$ crystals are assumed to be 30 mm thick. For comparison we also generated the count-rate curves for a GSO-based scanner which uses 20 mm thick crystals and has an axial FOV of 18 cm, very similar to the Philips *Allegro* scanner.

Table II compares the interaction probabilities for these two crystals. Note that 30 mm thick $LaBr_3$ has similar coincidence photo-peak efficiency as 20 mm thick GSO. We have shown that $4 \times 4 \times 30$ mm^3 $LaBr_3$ pixels produce high light output and good energy resolution, and assume that we will be able to achieve similar results with an array of crystals in a detector configuration. For GSO, we were more reluctant to increase the thickness because of cost, and because a small decrease in light output has a more measurable effect on energy resolution. To a good first approximation, the geometric sensitivity increases as the square of the axial FOV for an object which is longer than the axial FOV of the scanner. The geometric sensitivity for the $LaBr_3$ scanner is therefore a factor of $(25/18)^2 = 1.93$ higher than the GSO scanner. Hence, the overall sensitivity of the $LaBr_3$ scanner is $1.93 \times 0.22/0.26 = 1.63$ times the GSO scanner sensitivity (using numbers from Table II for coincidence efficiency).

Fig. 4 shows the true and NEC count-rates as generated through our HCRSim calculation. The GSO scanner was assumed to use a timing window of 8 ns, whereas the $LaBr_3$ is assumed to use a 6 ns timing window due to its better timing resolution The integration time in the GSO scanner was set at 120 ns as in the *Allegro* scanner. This is twice the GSO decay time of 60 ns and leads to an integration of 86% of collected light. Similarly, the integration time for the $LaBr_3$ scanner was also set set to twice its decay time (70 ns). The ELLD value was raised to 470 keV for $LaBr_3$ based upon the results in Fig. 3. For the GSO scanner, the ELLD value was 410 keV (same as currently implemented on *Allegro*). The energy resolution is assumed to be 19% and 6.7% for the GSO and $LaBr_3$ scanners, respectively. The GSO energy resolution is similar to that measured on our *Allegro* scanner. The 6.7% energy resolution at 511 keV for $LaBr_3$ is based upon the Montecrystal detector simulations as described in Section V. These simulations account for the additional loss in energy resolution due to light spreading within the lightguide, as well

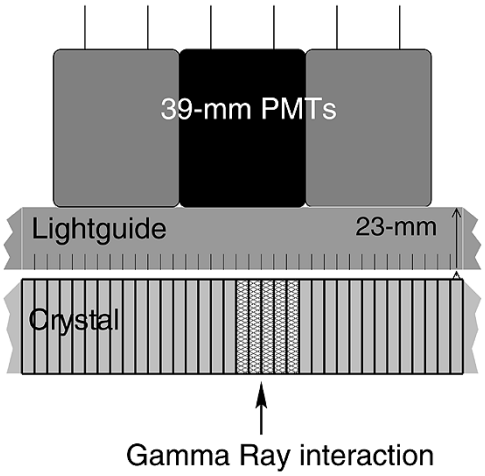

Fig. 5. Lateral view of an Anger logic detector using $4 \times 4 \times 30$ mm^3 crystals coupled to a continuous slotted lightguide and an array of 39 mm diameter PMTs. The lightguide thickness (t) is 2.3 cm, and the slots are 0.5 cm (s) deep. Five shaded crystals illustrate those illuminated by 511 keV photons for the data shown in Fig. 7.

as loss of light due to gaps between PMTs in a hexagonal array. For the 20 cm diameter by 70 cm long phantom (recommended by NEMA NU2–2001 for whole-body scanners), the calculated scatter fractions from the EGS4 Monte Carlo program are 25% and 16% for the GSO and $LaBr_3$ scanners, respectively. However, for the 40 cm by 70 cm phantom, representing a very large patient, the scatter fraction increases to 48% for GSO and 25% for the $LaBr_3$ scanners. Note that the NEC rates in Fig. 4 decrease for both scanners in moving from the 20 cm diameter to 40 cm diameter cylinder. However, the fractional decrease is much more significant for the GSO scanner (about a factor of 6) than for the $LaBr_3$ scanner (about a factor of 3). In summary, these curves indicate that the NEC improvement of the $LaBr_3$ scanner over the GSO scanner is about a factor of 2 for the 20 cm diameter phantom (slim patient) while the improvement is a factor of 4 for the 40 cm diameter phantom (heavy patient).

V. Crystal Discrimination in an Anger-Logic Detector

In addition to very high count-rate capability, we also expect $LaBr_3$ to have excellent spatial resolution. With $LaBr_3$ we can expect a total light output more than double that of NaI(Tl) (pulse clipped and normally integrated for 220 ns) and approximately five times that of GSO. We performed MonteCrystal [13], [14] simulations to calculate position spectra for $LaBr_3$ crystals. In these simulations, the path of an incoming gamma ray is traced until it undergoes either a photoelectric or Compton interaction in the crystal. Scintillation photons are generated at the point of interaction, and the path of each scintillation photon is traced until it either hits a PMT entrance window or exits the crystal without being detected. The detector is similar in design to the GSO Anger-logic detector with crystals coupled via a suitably thick, slotted lightguide to a hexagonal array of PMTs (see Figs. 5 and 6). The $LaBr_3$ crystals are $4 \times 4 \times 30$ mm^3 and the GSO crystals are $4 \times 4 \times 20$ mm^3, while the PMTs are 39 mm in diameter. A flood source illuminates a group of five crystals to produce the data shown in Fig. 7. These crystals span the center of one PMT to its edge.

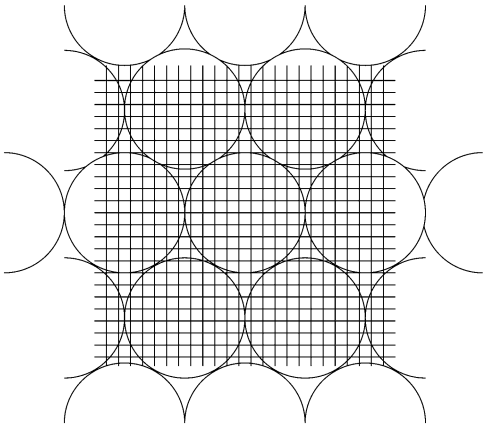

Fig. 6. Top view of the Anger-logic detector with crystals copuled to a heaxgonal array of PMTs via a lightguide.

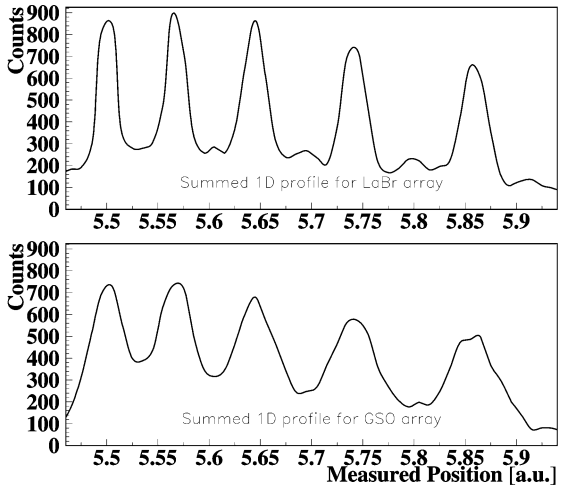

Fig. 7. Simulated position spectra for five adjacent crystals for (top) $LaBr_3$ compared to (bottom) GSO. Both detectors consist of 4 mm crystals coupled to a light-guide with an array of 39 mm diameter PMTs. One-dimensional profile spans the range from a PMT center to its edge.

Summed one-dimensional (1-D) profiles were then drawn to evaluate the crystal separation. As seen, the crystal separation achieved with $LaBr_3$ (Fig. 7, Top) is superior to GSO (Fig. 7, Bottom). In Table III we present results for accuracy of crystal positioning in these detector arrays for the Anger-positioning scheme after tracing the scintillation photons, and an energy weighted scheme which determines the interaction point based purely on the energy deposition in the crystal. The energy weighted scheme represents the ideal case of Anger positioning where one-to-one coupling exists between crystal and photo-detectors. These results show some degradation in accuracy of event positioning for GSO after Anger positioning is performed due to its lower light output. For $LaBr_3$, its higher light output reduces the probability of any further event localization errors. The final scanner resolution is also dependent on the ability of an automated crystal mapping algorithm which assigns interactions to individual crystals using a lookup table based upon a crystal flood image. With better crystal separation for $LaBr_3$, the accuracy of this algorithm is increased.

TABLE III
PERCENTAGE OF EVENTS CORRECTLY POSITIONED WITHIN THE INTERACTION CRYSTAL FOR GSO AND $LaBr_3$ DETECTORS USING ANGER-LOGIC POSITIONING AFTER SCINTILLATION LIGHT COLLECTION, AS WELL AS AN ENERGY WEIGHTED POSITIONING

	GSO	$LaBr_3$
Energy weighted (2D flood)	67%	49%
Anger positioning (2D flood)	64%	49%

Simulations have been performed for a point source in air placed within the GSO and $LaBr_3$ scanner designs to evaluate the reconstructed image resolutions. These simulations are based on EGS4 and include Compton scatter within the detector as well as the detector point spread function due to Anger logic positioning. Initial results show that the spatial resolution for a point source at the center of the scanner is 5.5/12.3 mm (fwhm/fwtm) and 5.3/9.7 mm for the $LaBr_3$ and GSO scanners, respectively. These results indicate that there is only a slight degradation in spatial resolution (at fwtm level) due to the lower photofraction of $LaBr_3$. Addtional simulations for a point placed radially away from the scanner center indicate similar results.

VI. TIMING RESOLUTION SIMULATION FOR A $LaBr_3$ ANGER-LOGIC DETECTOR

The timing resolution measured with an Anger-logic detector is a function of several factors besides the intrinsic timing resolution of the scintillator. Though our measurements indicate good intrinsic timing properties for the Lanthanum halide scintillators, it is important to evaluate the overall performance of an Anger detector using these scintillators. The timing resolution is now also a function of the crystal surface properties, its aspect ratio, and scintillation photon reflections within the crystal, the amount of Compton scatter in the crystal, the PMT transit time spread (TTS) or jitter, as well as transit time variations from a PMT photocathode center to its edge. The MonteCrystal simulations were once again utilized to perform event-by-event simulations for different arrangements of $4 \times 4 \times 30$ mm^3 $LaBr_3$ crystals. Best results were obtained when the four long surfaces had a specular finish. For each event a signal pulse was generated, and a subsequent analysis performed for timing pickoff.

For these calculations the PMT TTS was assumed to be 150 ps while a photocathode variation of 0.5 ns from PMT center to its edge was used. These values are typical for fast timing PMTs. Also, the crystal surface were modeled as specular or well-polished. Table IV lists the timing resolution calculated for a selection of detector configurations. The timing pickoff was calculated at 10% of the total integrated signal. The single crystal results are in general agreement with our measurements. These results show that with specular surfaces there is a small loss of timing resolution, as the crystal length increases, due to the high light output of $LaBr_3$. Using an array of $4 \times 4 \times 30$ mm^3 crystals in an Anger logic detector leads to some loss of collected light due to gaps between the PMTs packed in a hexagonal array. Hence, the timing resolution for the crystal array degrades to 440 ps.

TABLE IV
RESULTS FROM TIMING RESOLUTION SIMULATIONS USING MONTECRYSTAL

	Time resolution (FWHM) (ps)
$4 \times 4 \times 4$ mm^3 crystal on a PMT	346
$4 \times 4 \times 10$ mm^3 crystal on a PMT	343
$4 \times 4 \times 20$ mm^3 crystal on a PMT	355
$4 \times 4 \times 30$ mm^3 crystal on a PMT	372
$4 \times 4 \times 30$ mm^3 crystal array on a PMT via a lightguide	440

VII. TIME-OF-FLIGHT (TOF) SCANNER

The high light output and fast decay time of the Lanthanum scintillators, together with the ability to maintain good timing resolution in an Anger-logic detector, opens a very interesting possibility of measuring time-of-flight (TOF), which leads to less amplification of noise in the reconstruction process and better signal-to-noise in the reconstructed image. Instruments for TOF-PET and related reconstruction approaches were investigated intensively in the early 1980s, but the performance that was achievable at that time was limited by the available scintillator materials, since the crystals that were fast enough for TOF-PET, including BaF_2 and CsF had only low light output and poor energy resolution. A more recent examination of TOF-PET was addressed for LSO [15], measuring timing resolution from 300–475 ps depending on the size and shape of the crystal; the larger number corresponds to a crystal 30 mm in length. Our simulation and mesurement results also indicate that a timing resolution of under 450 ps is possible for the Lanthanum halide based Anger detector. As an example, let us assume a coincidence timing resolution of $\Delta t = 500$ ps between a pair of $LaBr_3$ detectors. This infers an uncertainty in position Δx of 7.5 cm, where $\Delta x = \Delta t/2c$. If we refer back to early investigations on TOF [16] the argument for TOF relied on an effective gain in sensitivity that was due to the reduction in noise propagation from the backprojection. Thus, the gain is expected to improve as the position uncertainty decreases, and as the diameter of the object increases. Here, we go through the TOF gain calculation in more detail, using the formalism of Strother [17] for SNR (signal-to-noise ratio).

In the early 1990s, Strother derived a formula for the SNR in a conventional PET scanner without TOF information, accounting for the presence of random and scatter coincidences [17]. In deriving this relationship, it was shown that the SNR was proportional to the square root of the NEC. We can use Strother's formulation to predict the gain in NEC achieved by using TOF information in a whole-body scanner, where the NEC already accounts for the decrease in noise due to reduction in randoms, which is another expected benefit from using a very fast scintillator.

The SNR of a reconstructed image element is [18]

$$\mathrm{SNR} = c\, t_e\, (\mathrm{VAR}_e)^{-1/2} \tag{1}$$

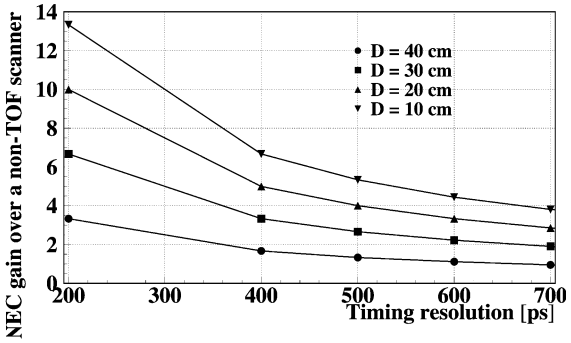

Fig. 8. Gain in NEC due to TOF measurement calculated as a function of timing resolution for varying cylinder diameters.

where c is a constant, t_e are the true coincidence counts in a reconstructed image element, and VAR_e is the weighted variance of the samples from each of the projection angles contributing to the image element. For a uniform cylinder, VAR_e is determined by the total number of counts in the image cells contributing to the projections. This is written as

$$\mathrm{VAR}_e = n_c\, t_e \tag{2}$$

where n_c is the number of image elements along the projection. With TOF information, the location of the annihilation point along the LOR is determined to within $\Delta x/2$ of the annihilation point and thus the number of image cells contributing to a given projection decreases to become

$$n_c = \frac{\Delta x}{d} \tag{3}$$

where d is the size of each image element. Note that without time-of-flight information, Δx is replaced with the diameter D of the cylinder. Substituting (2) and (3) into (1) gives

$$\mathrm{SNR} = c\left(\frac{d}{\Delta x}\right)^{1/2}(t_e)^{1/2}. \tag{4}$$

At this point in the calculation, we use Strother's derivation for t_e in terms of the total counts T, total scattered counts S, and total random counts R in the image. Thus the SNR ratio can now be written as

$$(\mathrm{SNR})_{\mathrm{TOF}} \propto \left(\frac{d}{\Delta x}\right)^{1/2}\left[\frac{T^2}{(T+Sc+R)}\right]^{1/2} \tag{5}$$

with the proportionality constant being a function of the cylinder and image matrix size. This definition reduces to the conventional (non-TOF) definition where Δx is replaced with the diameter, D, of the cylinder. Hence

$$(\mathrm{SNR})_{\mathrm{TOF}} = \left(\frac{D}{\Delta x}\right)^{1/2}(\mathrm{SNR})_{\mathrm{non-TOF}}. \tag{6}$$

These results are shown in Fig. 8 which is a plot of the gain in NEC (square of the SNR) for a scanner using TOF as a function of the timing resolution for varying object diameters, D. Returning to a $LaBr_3$ based whole-body scanner with TOF capability, a timing resolution of 500 ps would lead to a gain in SNR of 1.6 over a conventional PET tomograph for a 20 cm diameter cylinder. Looking at the NEC curves in Fig. 4 once more, we can conclude that the effective NEC rate of the $LaBr_3$-based whole-body scanner with an axial extent of 25 cm will be factor of 2.7 higher than that shown, reaching a peak$NEC \sim 120$ kc/s $\times\, 2.7 = 320$ kc/s, thus further distancing itself from the GSO-based scanner. For a larger object with $D = 40$ cm, more appropriate for a heavy patient, the SNR increase would be expected to be 2.3 with an NEC increase of 5.4 (peak$NEC \sim 40$ kc/s $\times\, 5.4 = 215$ kc/s). It is particularly beneficial that the TOF gain increases as the object size increases, since typically the NEC decreases for large patients due to increased attenuation and scatter. While these numbers may be optimistic, it is clear that the Lanthanum scintillator has a significant potential advantage in SNR, if we measure TOF. Unlike other scintillators used in the early 1980s for TOF (e.g., BaF_2 and CsF), $LaBr_3$ can be expected to have outstanding energy resolution and spatial resolution, as well.

VIII. Conclusion

In this work, we have shown that the excellent energy resolution, timing properties, and light output of Lanthanum halide scintillators can lead to the design of very high performance 3-D whole-body PET scanners. In particular, these scanners can lead to a factor of four improvement in the peak NEC for heavy patients over the new generation scanners using GSO as a scintillator. Additional simulations are underway for a detailed image quality analysis of a Lanthanum halide based scanner in comparison to a high density scintillator such as GSO or LSO. Initial results suggest that though there is a slight degradation in spatial resolution due to increased Compton scatter in the crystal, the better energy resolution of $LaBr_3$ will minimize scatter in the body and therefore lead to improved SNR in the images. Through some measurements and simulations, we also show that the timing resolution of these scitnillators can be maintained under 500 ps in an Anger-logic detector. This leads to the design for a 3-D PET tomograph with TOF measurement capability, which will be particularly important for heavy patient imaging.

References

[1] C. W. E. van Eijk, "Inorganic scintillators in medical imaging," *Phys. Med. Biol.*, vol. 47, pp. R85–R106, 2002.

[2] C. J. Thompson, Y. L. Yamamoto, and E. Meyer, "Positome II: A high efficiency positron imaging device for dynamic brain studies," *Trans. Nucl. Sci.*, vol. NS-26, pp. 583–589, Feb. 1979.

[3] K. Wienhard *et al.*, "The ECAT HRRT: Performance and first clinical application of the new high resolution research tomograph," *IEEE Trans. Nucl. Sci.*, vol. 49, pp. 104–110, Feb. 2002.

[4] J. S. Karp, S. Surti, R. Freifelder, M. E. Daube-Witherspoon, C. Cardi, L.-E. Adam, and G. Muehllehner, "Performance of a GSO PET camera," J. Nucl. Medicine, 2003, to be published.

[5] M. Moszyński, M. Kapusta, D. Wolski, M. Szawlowski, and W. Klamra, "Energy resolution of scintillation detectors: Readout with large area avalanche photodiodes and photomultipliers," *IEEE Trans. Nucl. Sci.*, vol. 45, pp. 472–477, June 1998.

[6] E. V. D. van Loef, P. Dorenbos, C. W. E. van Eijk, K. Kramer, and H. U. Gudel, "High-energy-resolution scintillator: Ce^{3+} activated $LaCl_3$," *Appl. Phys. Lett.*, vol. 77, pp. 1467–1468, 2000.

[7] ——, "High-energy-resolution scintillator: Ce^{3+} activated $LaBr_3$," *Appl. Phys. Lett.*, vol. 79, pp. 1573–1575, 2001.

[8] K. S. Shah *et al.*, "$LaBr_3$:Ce scintillators for gamma ray spectroscopy," *IEEE MIC Conf. Rec.*, p. N8-2, 2002.

[9] W. W. Moses, "Current trends in scintillator detectors and materials," *Nucl. Instrum. Methods*, vol. 487, pp. 123–128, 2002.

[10] S. Surti, J. S. Karp, and G. Muehllehner, "Evaluation of pixelated NaI(Tl) detectors for PET," *IEEE Trans. Nucl. Sci.*, vol. 50, pp. 24–31, Feb. 2003.
[11] D. A. Mankoff, G. Muehllehner, and J. S. Karp, "The high countrate performance of a two-dimiensionally position-sensitive detector for positron emission tomography," *Phys. Med. Biol.*, vol. 34, pp. 437–456, 1989.
[12] S. Surti, "A model of scintillation detector performance for positron emission tomography," Ph.D. dissertation, Univ. Pennsylvania, 2000.
[13] J. S. Karp and G. Muehllehner, "Performance of a position sensitive scintillation detector," *Phys. Med. Biol.*, vol. 30, pp. 643–655, 1985.
[14] S. Surti, J. S. Karp, R. Freifelder, and F. Liu, "Optimizing the performance of a PET detector using discrete GSO crystals on a continuous lightguide," *IEEE Trans. Nucl. Sci.*, vol. 47, pp. 1030–1036, June 2000.
[15] W. W. Moses and S. E. Derenzo, "Prospects for time-of-flight PET using LSO scintillator," *IEEE Trans. Nucl. Sci.*, vol. 46, pp. 474–478, 1999.
[16] T. F. Budinger, "Time-of-flight positron emission tomography: Status relative to conventional PET," *J. Nucl. Medicine*, vol. 24, pp. 73–78, 1983.
[17] S. C. Strother, M. E. Casey, and E. J. Hoffmann, "Measuring PET scanner sensitivity: Relating countrates to image signal-to-noise ratios using noise equivalent counts," *IEEE Trans. Nucl. Sci.*, vol. 37, pp. 783–788, 1990.
[18] G. L. Brownell, J. A. Correia, and R. G. Zamenhof, *Recent Advances in Nuclear Medicine*. New York: Grune Stratton, 1979.